

Dark-ages reionization and galaxy formation simulation–VII. The sizes of high-redshift galaxies

Chuanwu Liu^{1*}, Simon J. Mutch^{1†}, Gregory B. Poole¹, P. W. Angel¹, Alan R. Duffy²,
Paul M. Geil¹, Andrei Mesinger³ and J. Stuart B. Wyithe^{1‡}

¹*School of Physics, University of Melbourne, Parkville, VIC 3010, Australia*

²*Centre for Astrophysics and Supercomputing, Swinburne University of Technology, PO Box 218, Hawthorn, VIC 3122, Australia*

³*Scuola Normale Superiore, Piazza dei Cavalieri 7, I-56126 Pisa, Italy*

2 March 2022

ABSTRACT

We investigate high-redshift galaxy sizes using a semi-analytic model constructed for the Dark-ages Reionization And Galaxy-formation Observables from Numerical Simulation project. Our fiducial model, including strong feedback from supernovae and photoionization background, accurately reproduces the evolution of the stellar mass function and luminosity function. Using this model, we study the size–luminosity relation of galaxies and find that the effective radius scales with UV luminosity as $R_e \propto L^{0.25}$ at $z \sim 5$ –9. We show that recently discovered very luminous galaxies at $z \sim 7$ (Bowler et al. 2016) and $z \sim 11$ (Oesch et al. 2016) lie on our predicted size–luminosity relations. We find that a significant fraction of galaxies at $z > 6$ will not be resolved by *JWST*, but *GMT* will have the ability to resolve all galaxies in haloes above the atomic cooling limit. We show that our fiducial model successfully reproduces the redshift evolution of average galaxy sizes at $z > 5$. We also explore galaxy sizes in models without supernova feedback. The no-supernova feedback models produce galaxy sizes that are smaller than observations. We therefore conclude that supernova feedback plays an important role in determining the size–luminosity relation of galaxies and its redshift evolution during reionization.

Key words: galaxies: evolution – galaxies: formation – galaxies: high redshift – galaxies: fundamental parameters – galaxies: structure.

1 INTRODUCTION

The evolution of galaxy size during the Epoch of Reionization (EoR) provides an additional probe for understanding galaxy formation in the early Universe. In the hierarchical structure formation scenario (White & Rees 1978), dark matter haloes form first, then baryonic gas cools and falls into the potential well of dark matter haloes to form galaxies. Within this scheme, Fall & Efstathiou (1980) studied the formation of galaxy discs. In this model, the spin of a rotationally supported galaxy disc is gained from conservation of angular momentum during the collapse of cooling gas. Further analytic modelling by Mo et al. (1998) provided the relation between the disc scale of galaxy, R_d , and the virial radius of dark matter halo, R_{vir} , assuming an exponential

surface density profile

$$R_d = \frac{\lambda}{\sqrt{2}} \left(\frac{j_d}{m_d} \right) R_{\text{vir}}, \quad (1)$$

where m_d and j_d are the fraction of mass and angular momentum in the disc relative to the halo and λ is the spin parameter of the halo, which is a dimensionless measure of the angular momentum of the system. The proportionality with R_{vir} predicts that the sizes of discs scale with redshift by the inverse of the Hubble parameter, $H(z)^{-1}$ at a fixed circular velocity, or with $H(z)^{-2/3}$ at a fixed halo mass. Since $H(z) \propto (1+z)^{3/2}$ at high redshifts (Carroll et al. 1992), these predictions correspond to $(1+z)^{-3/2}$ and $(1+z)^{-1}$ respectively.

Observations of Lyman break galaxies (LBGs) show that galaxies are compact at higher redshift, and that average sizes evolves with redshift as $(1+z)^{-m}$ with $m \sim 1$ –1.5 (e.g. Ferguson et al. 2004; Bouwens et al. 2004; Oesch et al. 2010; Grazian et al. 2012; Ono et al. 2013; Kawamata et al. 2015; Holwerda et al. 2015; Shibuya et al. 2015).

Semi-analytic models have had considerable success

* chuanwul@student.unimelb.edu.au

† smutch@unimelb.edu.au

‡ swyithe@unimelb.edu.au

Table 1. Observed evolution of galaxy sizes, $R_e \propto (1+z)^m$ from literature, where $L_{z=3}^*$ corresponds to UV magnitude $M_{UV} = -21.0$.

z	m	Sources
$L = (0.3-1)L_{z=3}^*$		
2-6	1.05 ± 0.21	Bouwens et al. (2004)
2-8	1.12 ± 0.17	Oesch et al. (2010)
2-12	1.30 ± 0.13	Ono et al. (2013)
2.5-12	1.24 ± 0.10	Kawamata et al. (2015)
4-10	1.10 ± 0.06	Shibuya et al. (2015)
5-10	1.32 ± 0.43	Holwerda et al. (2015)
$L = (0.12-0.3)L_{z=3}^*$		
2-8	1.32 ± 0.52	Oesch et al. (2010)
2-12	1.30 ± 0.13	Ono et al. (2013)
4-10	1.22 ± 0.05	Shibuya et al. (2015)
5-10	0.76 ± 0.12	Holwerda et al. (2015)

studying the formation and evolution of galaxies in past two decades (e.g. White & Frenk 1991; Kauffmann et al. 1993; Cole et al. 2000; Croton et al. 2006; Bower et al. 2006; Lacey et al. 2011, 2015). The sizes of galaxies represent an important parameter in semi-analytic models, since the cold gas is assumed to settle in discs, where star formation occurs at a rate depending on the surface density (e.g. Croton et al. 2006). Reproducing the evolution of galaxy sizes in the early and dense Universe is therefore important for semi-analytic models of reionization. On the other hand, feedback mechanisms are already known to play an important role in suppressing star formation of galaxies.

Using the observed size evolution and the luminosity function of galaxies, Wyithe & Loeb (2011) presented a simple model to constrain galaxy sizes

$$R_e \propto L^{\frac{1}{3(1+a)}} (1+z)^{-m}, \quad (2)$$

where a and m are free parameters which can be constrained using both the slope of the galaxy luminosity function and galaxy size evolution.

Feedback could also affect the disc sizes through energy release and momentum outflow. Wyithe & Loeb (2011) ruled out the no-supernova feedback model at high confidence, and suggested a supernova feedback model through the transfer of momentum. Investigation of galaxy sizes using semi-analytic models have been made using galaxies in the both local and high redshift Universe (e.g. González et al. 2009; Shankar et al. 2010; Xie et al. 2015). Our purpose-designed semi-analytic model provides a tool to study the galaxy sizes during the EoR.

The semi-analytic model, MERAXES (described in Mutch et al. 2015, hereafter Paper-III), is a new purpose-built galaxy formation model designed for studying galaxy evolution during the EoR¹. MERAXES includes a temporally and spatially coupled treatment of reionization, and is built upon a high resolution and high cadence N -body simulation *Tiamat* (Poole et al. 2016, hereafter Paper-I). MERAXES

successfully reproduces a series of high-redshift galaxy observables including the stellar mass function (Paper-III) and UV luminosity function (Liu et al. 2015, hereafter Paper-IV). In this paper, we run simulations to investigate the size-luminosity relation, the size-stellar mass relation and the redshift evolution of galaxy sizes at $5 < z < 10$. We aim to use the evolution of galaxy sizes to probe the physics of galaxy formation during the EoR. In particular, We study how sensitive galaxy sizes are to feedback, especially from supernovae feedback during the EoR.

This paper is organized as follows. In Section 2 we briefly introduce the semi-analytic model and N -body simulation used in this work. In Section 3 we study the relation between sizes and UV luminosities of galaxies. In Section 5 we study the size-stellar mass relation of model galaxies. In Section 6 we present the predicted redshift evolution of galaxy sizes and compare this with observations. In Section 8, we present our conclusions. Throughout this work, we employ a standard spatially-flat Λ CDM cosmology based on *Planck* 2015 data (Planck Collaboration et al. 2015): $(h, \Omega_m, \Omega_b, \Omega_\Lambda, \sigma_8, n_s) = (0.678, 0.308, 0.0484, 0.692, 0.815, 0.968)$. All magnitudes in this paper are presented in the AB system (Oke & Gunn 1983). The unit of luminosity, $L_{z=3}^*$, is the characteristic luminosity at $z \sim 3$, which corresponds to $M_{1600} = -21.0$ (Steidel et al. 1999).

2 SIMULATION AND MODELLING

The galaxy formation model used in this work is MERAXES (Paper-III). MERAXES is implemented upon dark matter halo merger trees generated from the cosmological N -body simulation *Tiamat* (Paper-I). *Tiamat* and MERAXES have special features designed for the study of reionization.

2.1 N -body simulation

The collisionless N -body simulation, *Tiamat*, was run using a modified version of GADGET-2 (Springel 2005) and the *Planck* 2015 cosmology (Planck Collaboration et al. 2015). It includes 2160^3 particles in a comoving 100Mpc cube box. The mass of each particle is $2.64 \times 10^6 h^{-1} M_\odot$, which allows us to identify the low mass dark matter haloes close to the hydrogen cooling limit across the redshifts relevant to reionization. Dark matter halo finding was carried out using SUBFIND (Springel et al. 2001).

Tiamat outputs includes 100 snapshots from $z = 35$ to $z = 5$ with a temporal resolution of 11 Myr per snapshot. This high temporal resolution resolves the dynamical time of galaxy discs at high redshift, and is comparable to the lifetime of massive stars. Dark matter halo merger trees constructed from *Tiamat* are stored in a “horizontal” form. This allows the semi-analytic model to implement a self-consistent calculation of feedback from reionization on low mass galaxy formation.

2.2 Semi-analytic model

MERAXES is a new semi-analytic model based on Croton et al. (2006) with updated physics for application to $z > 6$. It consists of baryonic infall, gas cooling, star formation, stellar

¹ MERAXES model is a part of the Dark-ages Reionization And Galaxy-formation Observables from Numerical Simulation (DRAGONS) project, <http://dragons.ph.unimelb.edu.au>.

mass recycling, metal enrichment, galaxy mergers, gas stripings, and feedback from both supernova and reionization. To model the formation and evolution of galaxies during the EoR, MERAXES incorporates several improvements in the feedback scheme. Firstly, it considers a delayed supernova feedback mechanism. In an instantaneous feedback scheme, a massive star instantly produces a supernova and so releases its energy and mass within the same snapshot that the progenitor star formed. This is appropriate at low redshift, where the stellar lifetime is short compared to the galaxy dynamical time. However, our *Tiamat* merger trees have a much higher time resolution ~ 11 Myr, which is shorter than the lifetime of the least massive Type II supernova progenitor stars (e.g., ~ 40 Myr for $8 M_{\odot}$ stars). Therefore, MERAXES implements a delayed supernova feedback scheme, where a supernova may explode several snapshots after the progenitor star formed. MERAXES also includes feedback from a spatially and temporally variable ultraviolet background (UVB). The UVB radiation heats the intergalactic medium and reduces baryonic infall within small dark matter haloes, and suppresses the cooling and star formation. To achieve this, MERAXES integrates the semi-numerical code 21CMFAST (Mesinger et al. 2011) to construct the reionization structure.

We assume a standard Salpeter (1955) initial mass function (IMF) with stellar mass in the range of $0.1 < m_* < 120 M_{\odot}$:

$$\phi(m_*) \propto m_*^{-2.35}. \quad (3)$$

The free parameters in MERAXES were calibrated to replicate the observed stellar mass functions at $z \sim 5-7$ (González et al. 2011; Duncan et al. 2014; Grazian et al. 2015; Song et al. 2016) and the *Planck* optical depth to electron scattering measurements (Planck Collaboration et al. 2015). For a more detailed description of MERAXES, see Paper-III.

2.3 Disc sizes

In our semi-analytic model, we adopt the disc scale radius from Mo et al. (1998) as shown in Equation 1, and the standard assumption $j_d/m_d = 1$ (Fall & Efstathiou 1980), for which the specific angular momentum of the material which forms the disc is same to that of the host halo.

The spin parameter, λ is calculated from the N -body simulation using the definition (Bullock et al. 2001):

$$\lambda = \frac{J_{\text{vir}}}{\sqrt{2} M_{\text{vir}} V_{\text{vir}} R_{\text{vir}}}, \quad (4)$$

where M_{vir} and J_{vir} are mass and angular momentum enclosed within the virial radius², R_{vir} and $V_{\text{vir}} = \sqrt{GM_{\text{vir}}/R_{\text{vir}}}$ is the circular velocity at R_{vir} . (See Angel et al. 2016, for a discussion of spin parameters for haloes in *Tiamat*).

From Equations 1 & 4, we see that the disc sizes of galaxies are determined by the properties of dark matter haloes. We assume star formation and feedback processes do not directly modify the disc sizes. On the other hand,

² R_{vir} is defined as that within which the mean density is $\Delta = 18\pi^2 + 82(\Omega_m(z)-1) - 39(\Omega_m(z)-1)^2$ times of the critical density, ρ_c (Bryan & Norman 1998).

the size of the disc does play a fundamental role in the build up of galaxy stellar mass. The cold gas, which cools from the halo hot gas reservoir of the host FoF group, is assumed to fall into the galaxy hosted by the central halo. MERAXES assumes the cold gas settles in a rotational supported disc with an exponential surface density profile. There is a critical surface density for the disc, above which it can not maintain stability and will start forming stars. The critical density at a radius r is adopted from Kauffmann (1996) as

$$\Sigma_{\text{crit}}(r) = \Sigma_{\text{norm}} \left(\frac{V_{\text{vir}}}{\text{km s}^{-1}} \right) \left(\frac{r}{\text{kpc}} \right)^{-1} M_{\odot} \text{pc}^{-2}, \quad (5)$$

where $\Sigma_{\text{norm}} = 0.2$ is a free parameter in MERAXES. Stars are assumed to form within a maximum radius set to $R_{\text{disc}} = 3R_d$ based on the properties of the Milky Way (van den Bergh 2000). By integrating Σ_{crit} to $R_{\text{disc}} = R_d$, we obtain a critical mass of the disc

$$m_{\text{crit}} = 2\pi \Sigma_{\text{norm}} \left(\frac{V_{\text{vir}}}{\text{km s}^{-1}} \right) \left(\frac{R_{\text{disc}}}{\text{kpc}} \right) 10^6 M_{\odot}. \quad (6)$$

If the mass of cold gas in the disc, m_{cold} exceeds this threshold mass the stars will form with a star formation rate given by

$$\dot{m}_* = \alpha_{\text{SF}} \frac{m_{\text{cold}} - m_{\text{crit}}}{t_{\text{dyn}}^{\text{disc}}}, \quad (7)$$

where $\alpha_{\text{SF}} = 0.03$ is a free parameter describing the star formation efficiency and $t_{\text{dyn}}^{\text{disc}} = R_d/V_{\text{vir}}$ is the dynamical time of the disc. Through this star formation process, the disc size affects a series of galaxy properties including UV luminosities. The size-luminosity relation therefore becomes an important prediction of galaxy formation models.

We note that the star forming process is rather complicated. It is not only determined by the galaxy sizes but also by other effects including cooling, mergers and feedback. To study the role of supernova feedback in the build up of the size-luminosity (stellar mass) relation, we also run a simulation with the supernova feedback switched off. This no supernova model cannot reproduce the stellar mass function in detail, but is recalibrated to provide the stellar mass density at $z = 5$ (see Paper-III).

In this paper, to compare with observations we present the sizes of model galaxies using the physical effective radius, (i.e., half-light radius), R_e , within which half of the galaxy's luminosity is contained. Here R_e is estimated using $R_e = 1.678 R_d$, where the constant originates from the assumed exponential surface density profile and constant mass-to-light ratio.

2.4 UV luminosities

Luminosity is the most direct observable of high-redshift galaxies. We calculate the UV luminosities using stellar population synthesis. For each galaxy we obtain the stellar population components by tracking its star formation and merger history. We integrate the stellar populations with model spectral energy distributions (SEDs) calculated using STARBURST99 (Leitherer et al. 1999; Vázquez & Leitherer 2005; Leitherer et al. 2010, 2014) with a constant metallicity of $Z = 0.05 Z_{\odot}$. We do not include nebular components as they would not affect the UV luminosities of our model galaxies at these redshifts.

Table 2. The best-fitting parameters R_0 and β (Equation 8) for the model galaxies with UV magnitudes $M_{UV} < -14$ at $z \sim 5-10$.

z	R_0/kpc	β
5	1.17 ± 0.05	0.25 ± 0.02
6	0.80 ± 0.05	0.23 ± 0.02
7	0.61 ± 0.07	0.25 ± 0.04
8	0.53 ± 0.07	0.28 ± 0.04
9	0.42 ± 0.06	0.30 ± 0.04
10	0.45 ± 0.04	0.36 ± 0.03

To obtain the observed luminosities we apply a dust extinction model to each galaxy. We adopt a luminosity dependent dust model (e.g. Smit et al. 2012; Bouwens et al. 2015) which is based on the IRX- β relation from Meurer et al. (1999) and the observed luminosity- β relation from Bouwens et al. (2014). For more details about the galaxy photometric modeling see Paper-IV.

3 SIZE-LUMINOSITY RELATION

We first investigate the predicted relation between the physical size and UV luminosity of model galaxies. Fig. 1 shows the relation between the effective radius and UV magnitude M_{UV} for model galaxies at $z \sim 5-10$, where the UV magnitude M_{UV} is the dust-extincted luminosity at the rest-frame 1600 Å. We see that at $M_{UV} \lesssim -14$, galaxies with brighter UV luminosity tend to have larger sizes.

However, the effective radius does not significantly change with luminosity for the galaxies with luminosities $M_{UV} > -14$. This is because galaxies fainter than $M_{UV} \sim -14$ are located in the dark matter haloes of the minimum gas cooling mass. This is similar to the turnover at $M_{UV} \sim -14$ in the relation between UV luminosity and the mass of dark haloes found in Paper-IV. We see that at fixed luminosity, the size of galaxies grows from $z \sim 10-5$. We discuss the redshift evolution of galaxy sizes further in Section 6.

The relation between the galaxy size and luminosity is commonly fitted by

$$R_e = R_0 \left(\frac{L_{UV}}{L_0} \right)^\beta, \quad (8)$$

where R_0 is the effective radius at L_0 , and β is the slope. We set $L_0 = L_{z=3}^*$ which corresponds to $M_0 = -21$ (Steidel et al. 1999). This equation can be rewritten as

$$\log_{10} R_e = -0.4 \times \beta (M_{UV} + 21) + \log_{10}(R_0). \quad (9)$$

We linearly fit the $\log_{10}(R_e)$ - M_{UV} relation for galaxies brighter than $M_{UV} = -14.5$ at each redshift. The best-fitting values for R_0 and β at $z \sim 5-10$ are shown in Table 2.

We see that the slope of the size-luminosity relation, β , does not significantly change at $z \sim 5-9$ and has a median value of $\beta \sim 0.25$. This value agrees with observational studies for both local and high-redshift galaxies. For example, de Jong & Lacey (2000) found $\beta = 0.253 \pm 0.020$ for local spiral galaxies. Shen et al. (2003) derived a slope of $\beta \approx 0.26$ for the late-type galaxies from SDSS. Courteau et al. (2007) obtained $\beta = 0.321 \pm 0.010$ from local field and cluster spiral galaxies. Grazian et al. (2012) found $\beta = 0.3-0.5$ for LBGs at $z \sim 7$, while Holwerda et al. (2015) derived $\beta = 0.24 \pm 0.06$

using the Grazian et al. (2012) data. In addition, Huang et al. (2013) found $\beta = 0.22$ and 0.25 for the galaxies in GOODS and HUDF fields at $z \sim 4$ and $z \sim 5$ respectively. Finally Shibuya et al. (2015) investigated the galaxy effective radius from a large *Hubble Space Telescope* (HST) sample and obtained $\beta = 0.27 \pm 0.01$ at $z \sim 0-8$. They also showed that β does not significantly evolve over this redshift range. Our study predicts that the size-luminosity relation $R_e \propto L^{0.25}$ holds for galaxies with UV luminosity brighter than $M_{UV} \sim -14$ at $z \sim 5-10$.

For comparison with our simulation predictions we add observed R_e - M_{UV} relations from (Huang et al. 2013) at $z \sim 5$ and Shibuya et al. (2015) at $z \sim 5-8$, where the latter is calculated by us using the sizes data from Shibuya et al. (2015). Our results are in close agreement with the observations.

Recently, Oesch et al. (2016) found an unexpectedly luminous galaxy (GN-z11) at $z \sim 11$, which has $M_{UV} = -22.1 \pm 0.2$ and $R_e = 0.6 \pm 0.3$ kpc. In Mutch et al. (2016) we demonstrated that the properties of GN-z11 are in good agreement with the results of our model in terms of stellar mass, star formation rate and UV luminosities. We show GN-z11 in Fig. 1 and we find that it is in agreement with our predicted size-luminosity relation at $z \sim 10$.

The model predicted size-luminosity relation is also consistent with the analytic prediction (Equation 2) of Wyithe & Loeb (2011). In this work they considered a supernova feedback model where supernova-driven winds conserve momentum in the interaction with the galactic gas. This model results in a luminosity scaling of $a = 1/3$ which corresponds to $R_e \propto L^{0.25}$. While the model without supernova feedback yields $a = 0$ which corresponds to $R_e \propto L^{0.33}$.

To study the role of supernova feedback on the build up of galaxy sizes, we show the size-luminosity relation for the no supernova feedback model in Fig. 1 (red circles). The size-luminosity relation for the no supernova feedback model is also flat at $M_{UV} > -14$. This is because the minimum size is set by the mass scale of efficient cooling in both models. There is no clear difference between the fiducial and no supernova feedback model at $M_{UV} > -17$, where the accumulated effect from supernova feedback on star formation histories is not significant enough to be observed. However, at $M_{UV} < -17$, the median size of galaxies from the no supernova feedback model is notably smaller than the fiducial model. In other words, for same size galaxy, the no supernova feedback model results in a much brighter luminosity. We note that removing supernova feedback allows more stars to form, and so the model has been recalibrated to produce the correct stellar mass density at $z = 5$. The luminosity difference is $\sim 2-3$ mag at $z = 5-7$, which is larger than the ~ 1 mag difference at $z = 8-10$. This is also due to the correct galaxy mass only being achieved at $z = 5$.

The different size-luminosity relations from these two models arise because the supernova feedback in the fiducial model suppresses star formation rate and resulting a more gradual star-formation history. In contrast, galaxies without supernova feedback have much burstier star-formation histories and contain more young stellar populations which are UV bright. These effects are more significant at lower redshift due to the longer star-formation histories. We also ran a simulation with both supernova and reionization feedback mechanisms switched off. However, we found the result to be

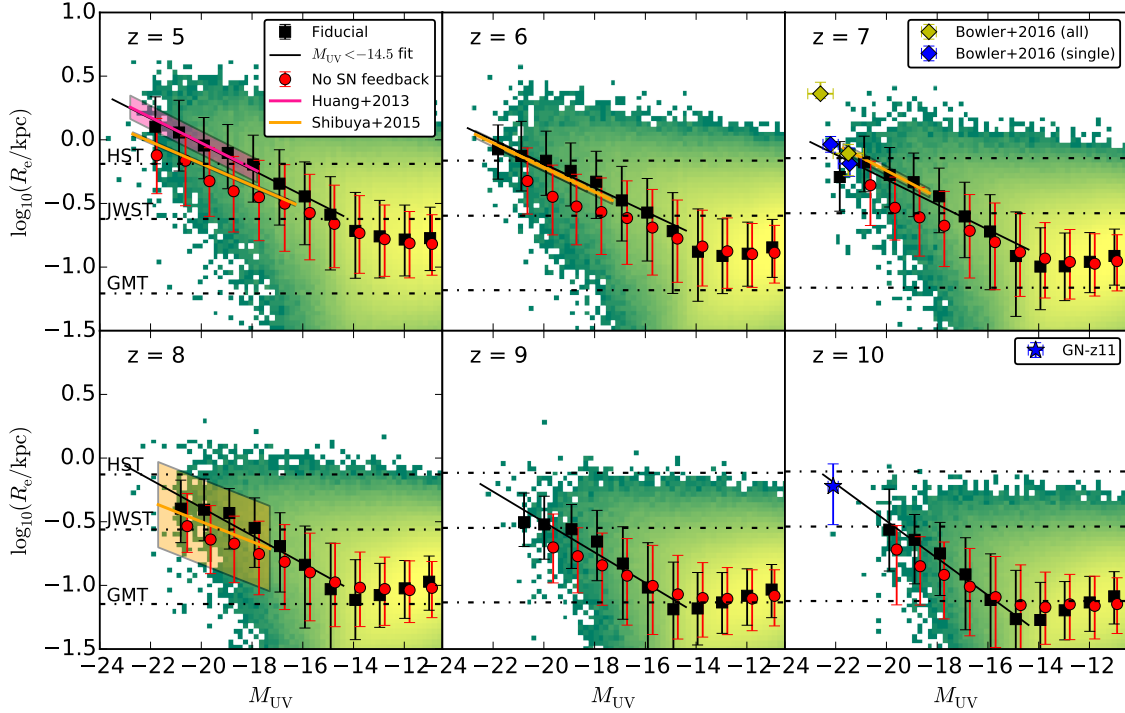


Figure 1. Effective radius of galaxies as a function of UV luminosity at $z \sim 5$ –10. The colour profile shows the logarithm density of the distribution. The black squares and error bars represent the median and 16th to 84th percentiles of the R_e distribution in bins which contain at least ten galaxies. The black solid lines are the linear best-fitting lines for galaxies with $M_{1600} < -14.5$. The pink and orange lines and associated shaded regions show the observed relations from Huang et al. (2013) and Shibuya et al. (2015). The blue and yellow diamonds show the observations at $z \sim 7$ from Bowler et al. (2016). The blue star shows luminous galaxy GN-z11 found by Oesch et al. (2016). For model comparison, the red circles and error bars show the median and distribution of size-luminosity from the model with supernova feedback turned off. The dash-dotted lines represent the angular resolution of *HST*, *JWST* and *GMT*.

almost identical to the no supernova feedback model, with only a tiny difference at lower redshifts ($z \sim 5$ –6).

4 RESOLVING GALAXIES WITH *HST*, *JWST* AND *GMT*

In Fig. 1 we show the spatial resolution of *Hubble Space Telescope* (*HST*), *James Webb Space Telescope* (*JWST*), and *Giant Magellan Telescope* (*GMT*)

$$\Delta r = \Delta \theta d_A = \frac{1.22\lambda}{D_{\text{tel}}} d_A, \quad (10)$$

where $\Delta \theta$ is the angular resolution determined by Rayleigh criterion, $\lambda = 1600(1+z)$ Å is the observed wavelength of UV photons, D_{tel} is the effective diameter of the telescope and d_A is the angular diameter distance. Any disc or distributed components smaller than Δr could not be resolved by the telescopes. In Equation 10, although the observed wavelength is scaled by a factor of $(1+z)$, the angular diameter distance decreases at a similar rate at $z \gtrsim 1$ so the spatial resolution does not rapidly change with redshift.

We see that *HST* ($D_{\text{tel}}=2.4$ m) can only resolve the brightest galaxies at $z \sim 5$ –6, and the structures of typical $z > 6$ galaxies can not be resolved. The larger diameter *JWST* ($D_{\text{tel}}=6.5$ m) will resolve galaxies brighter than

$M_{\text{UV}} = (-16, -18, -20)$ at $z = (6, 8, 10)$. However, with an exposure time $t_{\text{exp}} = 10^6$ s, *JWST* will observe galaxies to $M_{\text{UV}} = (-15.0, -15.8, -16.3)$ with the signal-to-noise ratio $S/N=10$ at these redshifts, hence a significant fraction of $z > 6$ galaxies will be unresolved. Due to the large mirror size, *GMT* ($D_{\text{tel}}=25$ m) will have the ability to resolve all galaxies in haloes above the atomic cooling limit.

5 MASS–SIZE RELATION

Fig. 2 shows the relation between the effective radius and stellar mass of galaxies at $z \sim 5$, 6, 8 and 10 for both fiducial and no supernova feedback models. Observed data from Mosleh et al. (2012) are also shown. The model size-mass relation is in good agreement with these observations. We see that for galaxies with stellar masses above $10^{6.5} M_{\odot}$, more massive galaxies tend to have larger sizes. The galaxies from the fiducial model have larger sizes than the galaxies from no supernova feedback model at fixed stellar mass. However, the difference in the size-mass relation between the fiducial and no supernova feedback model is much smaller than in the size-luminosity relation. This is expected because we have tuned both models to produce the galaxy stellar mass density. However, star formation histories including supernovae

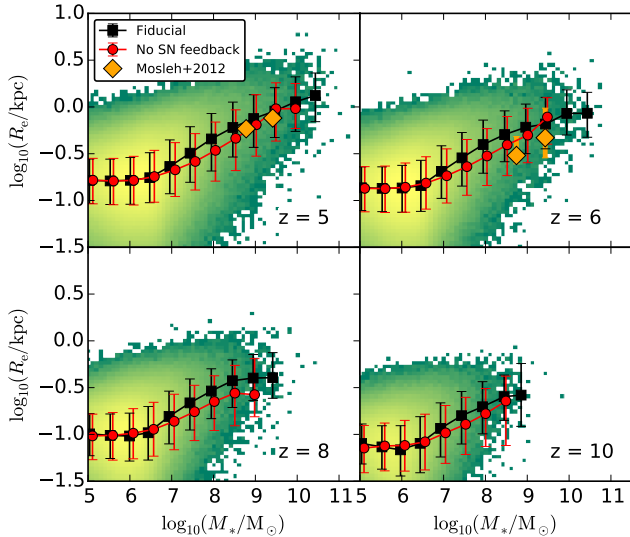


Figure 2. Size-mass relation of model galaxies at $z = 5, 6, 8, 10$. The colour profile shows the logarithm density of the distribution. The black squares and red circles show the median relation in bins which contain at least ten galaxies. The error bars represent the median and 16th to 84th percentiles of the intrinsic scatter. The orange diamonds show the observations from Mosleh et al. (2012)

lead to less variable UV luminosities resulting in larger difference seen in Fig. 1. For galaxies with $M_* < 10^{6.5} M_\odot$, our two models show similar galaxy sizes due to the inefficient star formation in the minimum cooling mass, as was the same case in the size–luminosity relation in Fig. 1.

6 REDSHIFT EVOLUTION OF SIZES

Apart from the luminosity dependence, the redshift evolution of galaxy sizes is another important measurement (e.g. Ferguson et al. 2004; Bouwens et al. 2004; Oesch et al. 2010; Grazian et al. 2012; Ono et al. 2013; Kawamata et al. 2015; Holwerda et al. 2015; Shibuya et al. 2015). Fig. 3 shows the predicted redshift evolution of the effective radius of galaxies. To compare with observations of size evolution, galaxies were selected using their luminosity in ranges of $(0.3-1)L_{z=3}^*$ and $(0.12-0.3)L_{z=3}^*$. These luminosity ranges correspond to UV magnitudes from -21.0 to -19.7 and from -19.7 to -18.7 respectively. Both fiducial and no supernova feedback models are shown in the figure. For comparison the observed galaxy sizes from Bouwens et al. (2004), Oesch et al. (2010), Ono et al. (2013), Kawamata et al. (2015), Holwerda et al. (2015) and Shibuya et al. (2015) are also shown.

We see that the evolution of galaxy sizes from our fiducial model is in good agreement with observations. The galaxy sizes in the no supernova feedback model are underestimated at each redshift, which is consistent with the results from the size–luminosity relation. To investigate the influence of parameter calibration in the no-supernova model, we also run an uncalibrated no-supernova feedback simulation and find a qualitatively similar result. Therefore, we

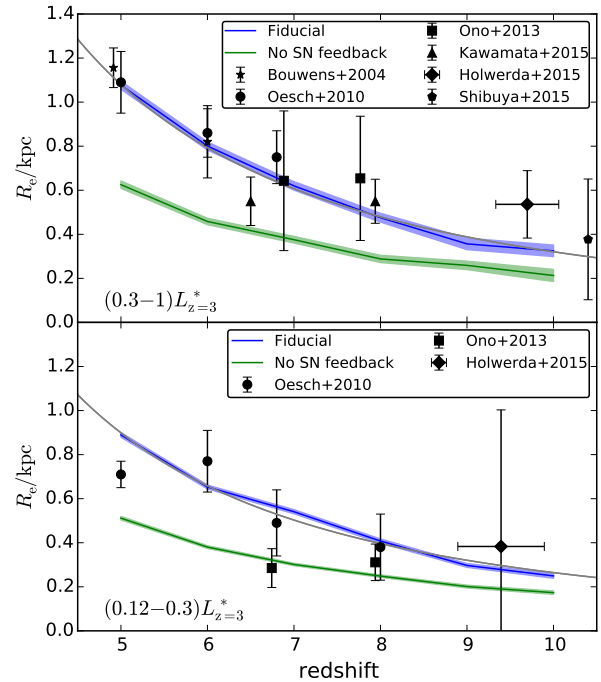


Figure 3. The redshift evolution of the mean effective radius for galaxies in the luminosity range $(0.3-1)L_{z=3}^*$ (upper panel) and $(0.12-0.3)L_{z=3}^*$ (lower panel). The blue line shows the mean effective radius from the fiducial model and the green line shows the mean effective radius from the model without supernova feedback. The shaded regions show the associated 1σ uncertainties of the means. The grey solid lines show the power law fit from our model predictions. For comparison, we show the observed mean sizes from Bouwens et al. (2004), Oesch et al. (2010), Ono et al. (2013), Kawamata et al. (2015), Holwerda et al. (2015) and Shibuya et al. (2015). We see that our fiducial model agrees with observations, while the no supernova model significantly underestimates the galaxy sizes.

conclude that the galaxy size evolution provides an additional observable for determining the importance of supernova feedback in early galaxy formation.

We fit the predicted size evolution at $z \sim 5-10$ using $R_e \propto (1+z)^{-m}$ and find $m = 2.00 \pm 0.07$ with $R_e(z=7) = 0.61 \pm 0.01$ kpc for galaxies with luminosity in the range $(0.3-1)L_{z=3}^*$ and $m = 2.02 \pm 0.04$ with $R_e(z=7) = 0.50 \pm 0.01$ kpc for galaxies with luminosity in the range $(0.12-0.3)L_{z=3}^*$. The fitted relations are shown as grey solid lines in Fig. 3. We also show $\Delta\chi^2 = 1$ confidence intervals using the observations from Bouwens et al. (2004), Oesch et al. (2010) and Ono et al. (2013), as well as combined observations from all data shown in Fig. 4. Here we only include the observational data at $z > 5$ and do not include more precise measurements at $z < 5$ which could dominate the fit.

We see that the predicted m from our model is comparable to observations. For example, $m = 1.64 \pm 0.30$ and $m = 1.82 \pm 0.51$ are derived by using combined observations shown in Fig. 4 with luminosities in the ranges $(0.3-1)L_{z=3}^*$

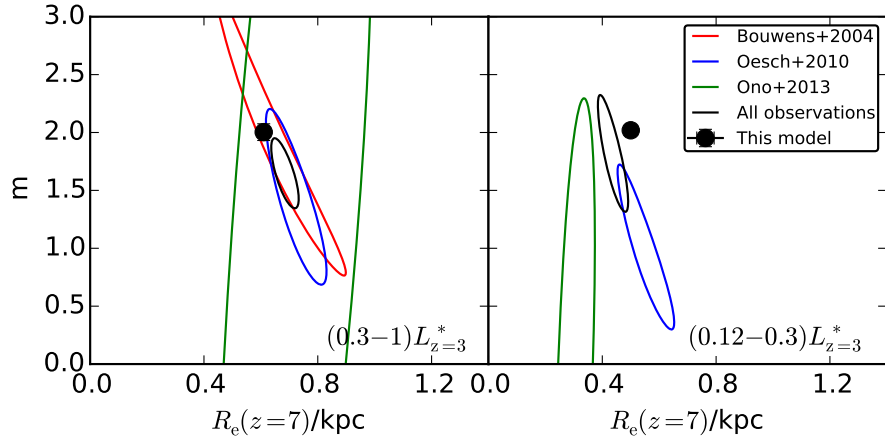


Figure 4. Confidence ellipses with $\Delta\chi^2 = 1$, which projects 1σ uncertainties on m and R_e axes. The red, blue and green contours are $z \gtrsim 5$ only observations from Bouwens et al. (2004), Oesch et al. (2010) and Ono et al. (2013) respectively. The black contours are from all observations shown in Fig. 3. Our model predictions are shown as black filled circles.

and $(0.12-0.3)L_{z=3}^*$ respectively. We note that the fits from our model as well as $z > 5$ observations give a larger values for m compared to observations including $z < 5$ data as shown in Table 1. This may suggest that galaxy sizes undergo a faster evolution at $z > 5$ compared to the evolution at lower redshift.

The normalization, $R_e(z=7)$ for model galaxies with luminosity in the range $(0.12-0.3)L_{z=3}^*$ is slightly larger than the combined observations. However, these $z > 5$ observations are also inconsistent with each other due to the large uncertainties from the small sample. We find that $R_e(z=7)$ is in agreement with combined observations with 3σ uncertainty.

7 MEASURE OF GALAXY SIZES

Before concluding, we discuss the applicability of R_e as a measure of galaxy sizes. In observations, morphologies of LBGs are often found to be irregular and clumpy, sometimes showing multiple components (e.g. Giavalisco et al. 1996; Ravindranath et al. 2006; Curtis-Lake et al. 2014; Shibuya et al. 2016; Guo et al. 2015; Bowler et al. 2016). This could be due to two different formation mechanisms: (i) galaxy interactions, such as mergers (e.g. Lotz et al. 2006; Overzier et al. 2008); (ii) distributed and clumpy star formation regions within same collapsing cloud due to instabilities (e.g. Goldader et al. 2002; Law et al. 2007; Dekel et al. 2009; Oesch et al. 2010; Jiang et al. 2013; Behrendt et al. 2016).

Morphological studies at very high redshift are more challenging. Shibuya et al. (2016) investigated the evolution of clumpy galaxies with large *HST* samples and found that the clumpy fraction increases from $z \sim 0$ to $z \sim 1$ but subsequently decreases from $z \sim 1-3$ to $z \sim 8$. On the other hand, high-resolution cosmological simulations show that galaxies at $z \gtrsim 6$ are dominated by disc morphologies (e.g. Pawlik et al. 2011; Romano-Díaz et al. 2011; Feng et al. 2015). For example, using the large-volume BLUETIDE simulation,

Feng et al. (2015) found that at $z = 8-10$, up to 70 per cent of the galaxy population more massive than $10^{10} M_\odot$ are disc galaxies. Detailed measurement of more compact and clumpy galaxies are limited by the angular resolution of instruments, and the origin of observed clumpy morphologies at high-redshift is still under debate.

Bowler et al. (2016) recently published size measurements for a sample of extremely luminous galaxies at $z \sim 7$. Bowler et al. (2016) divided the sample into two groups (single and multi-component) according to their morphologies. The size measurements are shown as the yellow (all galaxies) and blue (single component) diamonds in Fig. 1. We see that the size-luminosity relation for the single morphology galaxies is in good agreement with our model while including clumpy morphology galaxies leads to larger sizes. This may suggest that the multi-component galaxies are merging systems (Bowler et al. 2016). However, we are not able to rule out the clumpy-formation scenario due to the simplification of our semi-analytic model. Also, limited by the volume and mass resolution of our N -body simulation, the bright multi-component galaxies which undergo mergers will not be resolved by our model.

8 CONCLUSIONS

We have used the semi-analytic model MERAXES to study the dependence of galaxy sizes on UV luminosity, stellar mass and redshift at $z \sim 5-10$. We also studied the effect of supernova feedback on the evolution of galaxy sizes. We show that the rotationally supported disc model adopted in semi-analytic models can be used to study the sizes of high-redshift galaxies. Other primary findings are that:

(i) The effective radius scales with UV luminosity as $R_e \propto L^{0.25}$ for galaxies with luminosity $M_{UV} \lesssim 14$. Galaxies with the same disc size in the no supernova feedback model have brighter UV magnitudes than the fiducial model.

(ii) Our fiducial model with strong supernova feedback successfully reproduces the redshift evolution of average galaxy sizes at $z > 5$, which is slightly steeper than $z < 5$ observations. The model with no supernova feedback produces a significantly smaller radius at fixed luminosity than the fiducial model.

(iii) The recently identified luminous galaxy GN-z11 at $z \sim 11$ (Oesch et al. 2016) lies on our predicted size-luminosity relation. Our prediction is also in agreement with the size measurements of very luminous galaxies containing single components and with individual components of luminous multi-component systems at $z \sim 7$ (Bowler et al. 2016).

(iv) A significant fraction of $z > 6$ galaxies will not be resolved by *JWST*. However, *GMT* will have the ability to resolve all galaxies in haloes above the atomic cooling limit.

We conclude that galaxy sizes provide an important additional constraint on galaxy formation physics during reionization, and that current observations of galaxy size and evolution reinforce the importance of supernova feedback. These findings are in agreement with results based on the stellar mass function and luminosity function.

ACKNOWLEDGEMENTS

This research was supported by the Victorian Life Sciences Computation Initiative (VLSCI), grant ref. UOM0005, on its Peak Computing Facility hosted at the University of Melbourne, an initiative of the Victorian Government, Australia. Part of this work was performed on the gSTAR national facility at Swinburne University of Technology. gSTAR is funded by Swinburne and the Australian Governments Education Investment Fund. This research programme is funded by the Australian Research Council through the ARC Laureate Fellowship FL110100072 awarded to JSBW. AM acknowledges support from the European Research Council (ERC) under the European Unions Horizon 2020 research and innovation programme (grant agreement no. 638809 AIDA).

REFERENCES

- Angel P. W., Poole G. B., Ludlow A. D., Duffy A. R., Geil P. M., Mutch S. J., Mesinger A., Wyithe J. S. B., 2016, *MNRAS*, **459**, 2106
- Behrendt M., Burkert A., Schartmann M., 2016, *ApJ*, **819**, L2
- Bouwens R. J., Illingworth G. D., Blakeslee J. P., Broadhurst T. J., Franx M., 2004, *ApJ*, **611**, L1
- Bouwens R. J., et al., 2014, *ApJ*, **793**, 115
- Bouwens R. J., et al., 2015, *ApJ*, **803**, 34
- Bower R. G., Benson A. J., Malbon R., Helly J. C., Frenk C. S., Baugh C. M., Cole S., Lacey C. G., 2006, *MNRAS*, **370**, 645
- Bowler R. A. A., Dunlop J. S., McLure R. J., McLeod D. J., 2016, preprint, ([arXiv:1605.05325](https://arxiv.org/abs/1605.05325))
- Bryan G. L., Norman M. L., 1998, *ApJ*, **495**, 80
- Bullock J. S., Kolatt T. S., Sigad Y., Somerville R. S., Kravtsov A. V., Klypin A. A., Primack J. R., Dekel A., 2001, *MNRAS*, **321**, 559
- Carroll S. M., Press W. H., Turner E. L., 1992, *ARA&A*, **30**, 499
- Cole S., Lacey C. G., Baugh C. M., Frenk C. S., 2000, *MNRAS*, **319**, 168
- Courteau S., Dutton A. A., van den Bosch F. C., MacArthur L. A., Dekel A., McIntosh D. H., Dale D. A., 2007, *ApJ*, **671**, 203
- Croton D. J., et al., 2006, *MNRAS*, **365**, 11
- Curtis-Lake E., et al., 2014, preprint, ([arXiv:1409.1832](https://arxiv.org/abs/1409.1832))
- Dekel A., Sari R., Ceverino D., 2009, *ApJ*, **703**, 785
- Duncan K., et al., 2014, *MNRAS*, **444**, 2960
- Fall S. M., Efstathiou G., 1980, *MNRAS*, **193**, 189
- Feng Y., Di Matteo T., Croft R., Tenneti A., Bird S., Battaglia N., Wilkins S., 2015, *ApJ*, **808**, L17
- Ferguson H. C., et al., 2004, *ApJ*, **600**, L107
- Giavalisco M., Steidel C. C., Macchetto F. D., 1996, *ApJ*, **470**, 189
- Goldader J. D., Meurer G., Heckman T. M., Seibert M., Sanders D. B., Calzetti D., Steidel C. C., 2002, *ApJ*, **568**, 651
- González J. E., Lacey C. G., Baugh C. M., Frenk C. S., Benson A. J., 2009, *MNRAS*, **397**, 1254
- González V., Labbé I., Bouwens R. J., Illingworth G., Franx M., Kriek M., 2011, *ApJ*, **735**, L34
- Grazian A., et al., 2012, *A&A*, **547**, A51
- Grazian A., et al., 2015, *A&A*, **575**, A96
- Guo Y., et al., 2015, *ApJ*, **800**, 39
- Holwerda B. W., Bouwens R., Oesch P., Smit R., Illingworth G., Labbe I., 2015, *ApJ*, **808**, 6
- Huang K.-H., Ferguson H. C., Ravindranath S., Su J., 2013, *ApJ*, **765**, 68
- Jiang L., et al., 2013, *ApJ*, **773**, 153
- Kauffmann G., 1996, *MNRAS*, **281**, 475
- Kauffmann G., White S. D. M., Guiderdoni B., 1993, *MNRAS*, **264**, 201
- Kawamata R., Ishigaki M., Shimasaku K., Oguri M., Ouchi M., 2015, *ApJ*, **804**, 103
- Lacey C. G., Baugh C. M., Frenk C. S., Benson A. J., 2011, *MNRAS*, **412**, 1828
- Lacey C. G., et al., 2015, preprint, ([arXiv:1509.08473](https://arxiv.org/abs/1509.08473))
- Law D. R., Steidel C. C., Erb D. K., Pettini M., Reddy N. A., Shapley A. E., Adelberger K. L., Simenc D. J., 2007, *ApJ*, **656**, 1
- Leitherer C., et al., 1999, *ApJS*, **123**, 3
- Leitherer C., Ortiz Otálvaro P. A., Bresolin F., Kudritzki R.-P., Lo Faro B., Pauldrach A. W. A., Pettini M., Rix S. A., 2010, *ApJS*, **189**, 309
- Leitherer C., Ekström S., Meynet G., Schaerer D., Agienko K. B., Levesque E. M., 2014, *ApJS*, **212**, 14
- Liu C., Mutch S. J., Angel P. W., Duffy A. R., Geil P. M., Poole G. B., Mesinger A., Wyithe J. S. B., 2015, preprint, ([arXiv:1512.00563](https://arxiv.org/abs/1512.00563))
- Lotz J. M., Madau P., Giavalisco M., Primack J., Ferguson H. C., 2006, *ApJ*, **636**, 592
- Mesinger A., Furlanetto S., Cen R., 2011, *MNRAS*, **411**, 955
- Meurer G. R., Heckman T. M., Calzetti D., 1999, *ApJ*, **521**, 64
- Mo H. J., Mao S., White S. D. M., 1998, *MNRAS*, **295**, 319
- Mosleh M., et al., 2012, *ApJ*, **756**, L12
- Mutch S. J., Geil P. M., Poole G. B., Angel P. W., Duffy A. R., Mesinger A., Wyithe J. S. B., 2015, preprint, ([arXiv:1512.00562](https://arxiv.org/abs/1512.00562))
- Mutch S. J., et al., 2016, preprint, ([arXiv:1605.08054](https://arxiv.org/abs/1605.08054))
- Oesch P. A., et al., 2010, *ApJ*, **709**, L21
- Oesch P. A., et al., 2016, *ApJ*, **819**, 129
- Oke J. B., Gunn J. E., 1983, *ApJ*, **266**, 713
- Ono Y., et al., 2013, *ApJ*, **777**, 155
- Overzier R. A., et al., 2008, *ApJ*, **677**, 37
- Pawlik A. H., Milosavljević M., Bromm V., 2011, *ApJ*, **731**, 54
- Planck Collaboration et al., 2015, preprint, ([arXiv:1502.01589](https://arxiv.org/abs/1502.01589))
- Poole G. B., Angel P. W., Mutch S. J., Power C., Duffy A. R., Geil P. M., Mesinger A., Wyithe S. B., 2016, *MNRAS*, **459**, 3025
- Ravindranath S., et al., 2006, *ApJ*, **652**, 963

- Romano-Díaz E., Choi J.-H., Shlosman I., Trenti M., 2011, [ApJ](#), **738**, L19
- Salpeter E. E., 1955, [ApJ](#), **121**, 161
- Shankar F., Marulli F., Bernardi M., Boylan-Kolchin M., Dai X., Khochfar S., 2010, [MNRAS](#), **405**, 948
- Shen S., Mo H. J., White S. D. M., Blanton M. R., Kauffmann G., Voges W., Brinkmann J., Csabai I., 2003, [MNRAS](#), **343**, 978
- Shibuya T., Ouchi M., Harikane Y., 2015, [ApJS](#), **219**, 15
- Shibuya T., Ouchi M., Kubo M., Harikane Y., 2016, [ApJ](#), **821**, 72
- Smit R., Bouwens R. J., Franx M., Illingworth G. D., Labbé I., Oesch P. A., van Dokkum P. G., 2012, [ApJ](#), **756**, 14
- Song M., et al., 2016, [ApJ](#), **825**, 5
- Springel V., 2005, [MNRAS](#), **364**, 1105
- Springel V., White S. D. M., Tormen G., Kauffmann G., 2001, [MNRAS](#), **328**, 726
- Steidel C. C., Adelberger K. L., Giavalisco M., Dickinson M., Pettini M., 1999, [ApJ](#), **519**, 1
- Vázquez G. A., Leitherer C., 2005, [ApJ](#), **621**, 695
- White S. D. M., Frenk C. S., 1991, [ApJ](#), **379**, 52
- White S. D. M., Rees M. J., 1978, [MNRAS](#), **183**, 341
- Wyithe J. S. B., Loeb A., 2011, [MNRAS](#), **413**, L38
- Xie L., Guo Q., Cooper A. P., Frenk C. S., Li R., Gao L., 2015, [MNRAS](#), **447**, 636
- de Jong R. S., Lacey C., 2000, [ApJ](#), **545**, 781
- van den Bergh S., 2000, *The Galaxies of the Local Group*. Cambridge

This paper has been typeset from a $\text{\TeX}/\text{\LaTeX}$ file prepared by the author.